

**CHARACTERISATION OF A GIMBAL'S RESPONSE WHEN ATTACHED  
TO A DRONE TO ROLL, PITCH AND YAW MOVEMENTS OF A DRONE**

Oliver Aston George Silk

Bachelor of Engineering  
Mechatronic Engineering



Department of Electronic Engineering  
Macquarie University

June 5, 2017

Supervisor: Dr. David Inglis



## **ACKNOWLEDGMENTS**

I would like to acknowledge and thank Dr. David Inglis for his continuing support and guidance during both my University career and thesis. His mentoring and effective feedback has been invaluable in the progress and completion of this thesis.

Furthermore, I wish to acknowledge the efforts of Adrian Orellana, who designed and constructed the Sensor Suite for his thesis, and which I have used for the experiments in this thesis.





## **STATEMENT OF CANDIDATE**

I, Oliver Silk, declare that this report, submitted as part of the requirement for the award of Bachelor of Engineering in the Department of Mechatronic Engineering, Macquarie University, is entirely my own work unless otherwise referenced or acknowledged. This document has not been submitted for qualification or assessment at any academic institution.

Student's Name: Oliver Aston George Silk

Student's Signature:

Date: 05/06/2017



## ABSTRACT

With the increased capability of drones, comes the increased need for the ability to attach level sensitive packages and fly whilst these packages remain in a horizontal and leveled position. This thesis looks into the characteristic response of a horizontal and leveling gimbal device when used with a sensor suite consisting of two pairs a vector magnetometers. The project centres on the idea of using the gimbal to keep a sensor suite of vector magnetometers leveled, while connected to a low flying drone for meteorite detection. However, the scope of this device goes beyond that, looking into its applications in UXO detection and forensic geoscience.

The project incorporates testing methods with the goal of analysing and commenting on the characteristic response of a gimbal. To accomplish this, a mechanical lever apparatus was constructed to simulate a step input change of the drone's roll movement for the reason of testing a gimbal's response. The response of the gimbal was captured using a high speed camera, and then analysed over a sequence of frames using image processing software. The effect of the amplitude of the input angle change and added centralised mass onto the gimbal camera mount are explored through the comparison of the gimbal response's Overshoot, Settling time ( $T_s$ ) and Steady State Error ( $SSE$ ) during testing.



# Contents

Acknowledgments	iii
Abstract	vii
Table of Contents	ix
List of Figures	xiii
List of Tables	xv
<b>1 Introduction</b>	<b>1</b>
1.1 Introduction . . . . .	2
1.2 Project Overview . . . . .	2
1.3 Objectives . . . . .	3
1.3.1 Technical Objectives . . . . .	3
1.3.2 Gimbal Design Objectives . . . . .	3
1.3.3 Testing Device Design Objectives . . . . .	4
1.3.4 Scope of this Project . . . . .	4
<b>2 Literature Review</b>	<b>5</b>
2.1 Meteorites . . . . .	6
2.1.1 Current Methods for Meteorite Recovery . . . . .	6
2.2 Unexploded Ordinances . . . . .	7
2.3 Forensic Geophysics . . . . .	7
2.4 Magnetometer . . . . .	8
2.5 Planar Magnetic Gradiometers . . . . .	9
2.6 Mass Moment of Inertia . . . . .	9
2.6.1 Parallel-Axis Theorem . . . . .	10
2.6.2 Roll, Tilt and Pan . . . . .	11
2.7 Signals and Modern Control Theory . . . . .	12
2.7.1 Step Input . . . . .	12
2.7.2 Output Response . . . . .	12
2.7.3 Image Pixel Co-ordinates . . . . .	14

<b>3</b>	<b>Project Methodology</b>	<b>15</b>
3.1	Methodology Introduction . . . . .	15
3.2	Phase One . . . . .	16
3.2.1	Resource Requirements . . . . .	16
3.2.2	Moments of Inertia of the Sensor Suite . . . . .	16
3.2.3	Gimbal Selection . . . . .	17
3.2.4	Comparison . . . . .	17
3.3	Feiyu Gimbal Software . . . . .	17
3.3.1	Feiyu On . . . . .	18
3.3.2	Mounting the Sensor Suite to the Gimbal . . . . .	18
3.3.3	Variable Weight System . . . . .	19
3.4	Phase Two . . . . .	21
3.4.1	Resource Requirements . . . . .	21
3.4.2	Testing Device Requirements . . . . .	21
3.4.3	Testing Device Construction . . . . .	22
3.5	Phase Three . . . . .	26
3.5.1	Phantom Miro LC 320s . . . . .	26
3.5.2	Phantom Camera Control Software (PCC2.8) . . . . .	26
3.5.3	ImageJ Software . . . . .	27
3.5.4	MTrackJ . . . . .	27
3.5.5	Accounting for Uncertainty . . . . .	30
<b>4</b>	<b>Gimbal Response to Simulated Step-Response Experiment</b>	<b>31</b>
4.1	Gimbal Response Introduction . . . . .	31
4.1.1	Input Wave . . . . .	32
4.1.2	Failed tests . . . . .	32
4.1.3	Image Blur . . . . .	33
4.1.4	Drifting . . . . .	33
4.1.5	Response Wave Overshoot . . . . .	34
4.1.6	Response Wave Settling Time . . . . .	34
4.1.7	Response Wave Steady-State Error . . . . .	34
4.2	Experiments . . . . .	35
4.2.1	Experiment One . . . . .	35
4.2.2	Experiment Two . . . . .	37
4.2.3	Experiment Three . . . . .	39
4.2.4	Experiment Four . . . . .	41
4.3	Results . . . . .	43
<b>5</b>	<b>Discussion</b>	<b>45</b>
5.1	Broken Roll Motor . . . . .	45
5.2	Effect of Input wave . . . . .	45
5.3	Effect of Mass on the Gimbal's Response . . . . .	46
5.4	Effect of Angle change on Gimbal's Response . . . . .	47

*CONTENTS* xi

---

5.5 Gimbal's Response to movements in Pitch and Yaw . . . . .	47
<b>6 Conclusion</b>	<b>49</b>
<b>A Sensor Suite Roll, Pitch and Yaw Inertia</b>	<b>51</b>
<b>Bibliography</b>	<b>54</b>





## List of Figures

2.1	The potential search techniques success probability in different Environments. Black meaning high, shaded means medium and white means poor	8
2.2	The results from a drone assisted magnetometer survey [11]	9
2.3	CAD of the Feiyu MG Lite	11
2.4	Comparison of theoretical and real Step Inputs [7]	13
2.5	Unit Step Response [7]	14
2.6	Pixel coordinates [8]	14
3.1	a) Plastic Plate on top of sensor suite b) Sensor Suite attached to Bottom of Gimbal Camera Mount	18
3.2	Attached Hose clamps for use of Weight system	19
3.3	a) Aluminium Frame Plate b) Attached Aluminium Pieces to Frame Plate	23
3.4	a) Mounted testing device. b) Attached Extension Spring and Sponge	24
3.5	Experiment Setup	24
3.6	Cine Options	26
3.7	Saved Data Point	27
3.8	a) Multiple point Tracking b) Finished Track	28
3.9	MTrackJ Measure Tab	29
4.1	Exp3a Gimbal Arm Angle Change	32
4.2	The after shadow effect on a frame	33
4.3	Drift upward of the Sensor Arm in Exp4b	33
4.4	Exp 1c Simulation	36
4.5	Exp 1c Response	36
4.6	Exp 2a Simulation	38
4.7	Exp 2a Response	38
4.8	Exp 3a Simulation	40
4.9	Exp 3a Response	40
4.10	Exp 4a Simulation	42
4.11	Exp 4a Response	42
4.12	Bar Graph of Experiment Overshoot and Steady State Error	43
4.13	Bar Graph of Experiment Settling Time	43
A.1	Sensor Suite	52

A.2 Roll, Pitch and Yaw Moments of Inertia of the Sensor Suite . . . . .	53
--	----

## List of Tables

2.1	X,Y and Z axis inertia formulas for basic 3D shapes . . . . .	10
2.2	Definitions of Signals and Control Theory Terms . . . . .	12
3.1	Comparison of Ikan DS1 and the Feiyu MG Lite Specs . . . . .	17
3.2	Masses for the parts used in the weight system . . . . .	19
4.1	Table of Successful Tests . . . . .	32
4.2	Condition of Tests . . . . .	35
4.3	Results from Experiment One . . . . .	35
4.4	Results from Experiment Two . . . . .	37
4.5	Results from Experiment Three . . . . .	39
4.6	Results from Experiment Four . . . . .	41



# Chapter 1

## Introduction

## 1.1 Introduction

This thesis paper investigates the use of a gimbal for means of stabilization and leveling of a planar magnetic gradiometer sensor suite, mounted on the bottom of a drone for the purpose of near-surface meteorite detection in the Australian desert. The susceptibility of vector dependent sensors to changes in orientation, have created the need to horizontally level and stabilize a sensor suite when attempting to locate a meteorite. When flying over a meteorite, upon detection, the drone would save the coordinates, which would be available upon retrieval of the drone. If successful, this method would effectively replace current techniques, greatly diminishing labour and resource costs whilst increasing retrieval rates for meteorite collection.

The applicability of the gimbal stabilizing project goes beyond the initial scope of the project, and could establish a method which could be utilised in several industries that use planar magnetic gradiometers, or planar gravity gradiometers for surveying. Applications include Unexploded Ordinance (UXO) detection, geological and agricultural surveys, and forensic geoscience.

## 1.2 Project Overview

In completion of the thesis, the project was divided into three phases;

1. Phase One of the project included the integration of the gimbal with the magnetic sensor suite as well as calculations of the sensor suite's moments of inertia along its roll, pitch and yaw axis. This will determine whether the gimbal is capable of stabilizing and leveling when the sensor suite is attached, and for predictions of the effect of drone pitch and yaw movements to the gimbal's tilt and pan response later in the thesis. To attach the sensor suite, the sensor suite was mounted to the bottom of the gimbal using nuts and bolts.
2. Phase Two includes the design and manufacture of a lever testing device that was measure the characteristics of the gimbal's response. The testing device allows for the simulation of a step response of a drone moving from  $0 - 25^\circ$ .
3. During Phase Three the response of the gimbal to simulated drone movements was filmed using a high speed camera. The film will be separated into a sequence of frames, and the angle change sensor suite determined using image processing software. Data collected from the image processing software will then be exported into excel. Using the results, three variables; Overshoot, Settling Time ( $T_s$ ), and Steady State Error ( $SSE$ ) will be calculated.

## 1.3 Objectives

The following subsections describe the Technical and Design objectives of the project.

### 1.3.1 Technical Objectives

The technical objective of this research project was to determine the characteristic response of a gimbal system to a shift in roll, pitch or yaw. Due to the inertial mass of the sensor system discussed later in this document, the maximum load of the gimbal should be at least twice the weight of the sensor suite in order to ensure quality of the system's response to changes in roll.

To accomplish the project, an over the shelf gimbal was inverted and a magnetic sensor suite mounted to the bottom of the gimbal's camera mount. Rapid changes in angle were applied using a mechanical lever testing device and the gimbal's response was recorded using a High Speed Camera. The construction of the mechanical lever device is outlined in 3.4.3.

Taking into account the restrictions on weight that the drone could carry, and the inertial mass of the sensor suite, it was calculated that the gimbal and sensor suite combination had to weigh less than 3kg, with a weight of 1.5kg or less desirable to maximise the drone's battery life.

The primary operational environment for the drone system will be the Australian landscape. Due to the scorching conditions, the gimbal will have to operate in conditions of 50+° Celsius.

### 1.3.2 Gimbal Design Objectives

The design objectives are resulted from the harsh operating climate, the previous selection of the drone by the Department of Earth and Planetary, and the design of the Sensor Suite by Adrian Orellana. The key design requirements are that the gimbal should be:

1. Durable enough to withstand impact with shrubs and bushes.
2. Able to perform in temperatures of 50+°.
3. Lightweight such that it can be easily carried by the drone whilst not having a significant impact on the drone's performance nor its battery life.
4. Able to effectively handle the mass of the sensor suite with minimal sacrifice to the speed response and battery life.
5. Keep the sensor suite leveled within 2° of the desired orientation.

### 1.3.3 Testing Device Design Objectives

The design objectives for the testing apparatus are reflective of the physical demands of holding the gimbal handle, and simulating a step change in a drone's pitch. The key design requirements for the testing device are that it should be:

1. Capable of supporting the weight of the gimbal and mounted sensor suite.
2. Able to perform the change in desired angle within 0.3 seconds
3. Able to settle within the  $1^\circ$  of the desired angle within 0.7 seconds.
4. Able to grip the gimbal handle such that no slippage occurs.
5. Able to simulate a step change in roll.
6. Durable enough to withstand repeated testing.

#### Research Objective

The primary aim of this research project is to determine the characteristic response of a gimbal to a step change in its roll, pitch and yaw while carrying a sensor suite boom. The performance of the gimbal's response will be measured through testing and calculating its overshoot, settling time and steady state error. During testing the gimbal's added central mass and the amplitude of the step change angle will be varied, to discover the effect these variables have on the gimbal's response.

### 1.3.4 Scope of this Project

The main purpose for this thesis is for the localization and detection of meteorites. However uses of the sensor suite could just as easily be established for UXO detection or forensic geoscience means. Applications of the stabilizing and leveling device could extend beyond the use of sensor suites. The gimbal could assist with a drone's delivery of sensitive materials.



## **Chapter 2**

### **Literature Review**

## 2.1 Meteorites

The localization and identification of Australian meteorites is of high scientific interest [10]. Due to meteorites being the only source of extra-terrestrial material available for scientists [6], high quality meteorites are a unique source of information, providing scientists with their best glimpse into the earliest history of the solar system [12] [5]. Therefore, the creation of a more efficient and effective localization and detection technique is both important and beneficial.

### 2.1.1 Current Methods for Meteorite Recovery

The most common and widely used technique for meteorite location is through a visual search or hand-held magnetometers [9, 18]. This technique involves a team of scientists systematically line searching wide areas in a grid searching pattern. This method is often uneconomical, as it is labor and resource intensive often leading to no discovery. Increasing the tasks difficulty, is the hazardous desert environment that is most suitable for meteorite preservation, inhospitable to human habitation. In addition, space agencies seeking to recover solar system materials have spent billions of dollars on recovering meteorites [16] and now seek more cost-effective solutions.

An Autonomous vehicle named the Nomad Rover was the first of its kind to be designed and built for the goal of localization and detection of meteorites in 1997. Its successful first mission in Antarctica, 1998 [18] [17], led it to be used in subsequent missions the years after, where it managed to locate and classify a small amount of meteorites [6].

Nomad Rover uses image colour comparison to locate potential meteorites on the ice's surface [6]. This method is unsuitable for use in a desert environment as the camera is less effective, and the natural environment of the desert includes many non-meteorite rock that would need to be checked by the Nomad.

More recent techniques for meteorite localization include hyper-spectral imaging and the Fireball Network which has been operational since 2005. The Fireball is a network of cameras that capture a meteorite's fireball, to determine the trajectory of the incoming meteorite [16]. By using this technique with adequate observatory spacing, the trajectory triangulation can predict the fall to approximately 100m. However, uncertainty occurs during the dark flight of the meteorite, when no fireball is present. Due to uncertainties in the meteorite's mass, shape, and size which affect trajectory, the resting location of the meteorite is calculated with uncertainties.

A UAV drone magnetic boom would be ideal to use in conjunction with the Fireball Network. Using the results of the Fireball networks predicted trajectories, search areas could be minimised to within  $100m^2$ . This would allow for the drone to complete its search in just over thirty minutes, when traveling at  $5m/s$ .

## 2.2 Unexploded Ordinances

An Unexploded Ordinance or UXO is an explosive device that has not yet detonated. Devices that fall into this category include but are not limited to bombs, land or naval mines, shells and other explosive materials. An estimated 84 countries and 200,000km<sup>2</sup> of landmass is contaminated by landmines and UXOs [21]. These devices can often lie in agricultural lands and infrastructure, and their detonation can lead to loss of limbs, hearing loss, shrapnel wounds and death [15].

Currently, the most severely affected countries include those areas affected by the Vietnam war and second Indochina war, mainly Myanmar, Laos and Vietnam, as well as countries with more recent warfare, such as Afghanistan, Iraq, Egypt and Syria. However, reports of UXOs dating back to World War 2 are less common, but not unheard of.

In Laos, less than 1.25 Percent of estimated UXOs have been cleared, with over 20,000 killed or injured since the end of the Vietnam War era. More recently, UXOs still have a huge impact, killing or maiming over 1,000 individuals in Indochina countries per year [22]. Victims mostly stem from the poorest of the population, living in rural areas. With the high death rates still occurring, discovery and controlled detonation of these devices remains of high importance to many governments around the world.












































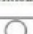



























### Magnetometry for UXO location

Magnetometry is one of the most efficient and cost-effective methods for locating UXOs. Magnetometers mounted on Unmanned Aerial Vehicles have been utilized by the American military for the use of UXO detection. Challenges faced by UAV drone UXO detection are perhaps even more difficult than normal methods, as many environments that UXOs are hidden in, are inaccessible, including underwater and in dense forest and bushland.

## 2.3 Forensic Geophysics

Electro-magnetic (EM) methods are commonly used by geophysicists in initial field tests, as they are cheap and relatively quick [14]. An object buried in the upper metre of earth can be detected with a magnetometer, which have often been used in searches for metallic weapons, clandestine graves and archaeological remains.

The technique is just one method that forensic scientists use, which includes electrical resistivity, electrical conductivity and Ground Penetrating Radar (GPR). When contemplating use of EM methods, scientists need to consider the potential for success by establishing the effect of the environmental conditions and the target item on their search technique [1].

Target(s)	Near-Surface Geophysics						
	Soil Type: Sand  Clay	Seis- mology /	Cond- uctivity	Resist- ivity	GPR	Mag- netics	Metal Detector
Unmarked Grave(s)							
Clandestine Grave(s)							
UXOs/ IEDs							
Weapons							
Drug/Cash Dumps							
Illegal Waste							
Common Depositional Environment							
Woods							
Rural							
Urban							
Coastal							

**Figure 2.1:** The potential search techniques success probability in different Environments. Black meaning high, shaded means medium and white means poor

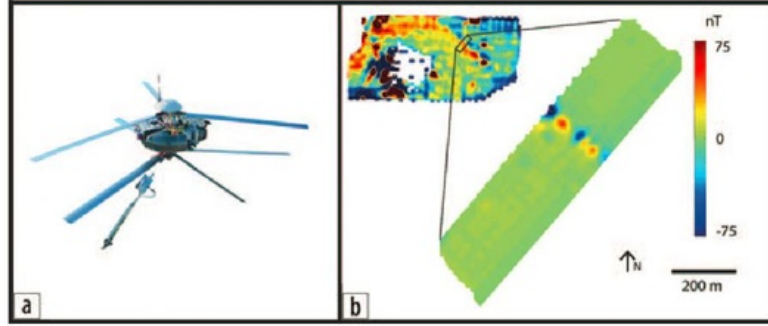
Figure 2.1 shows the success rates of different search techniques for targets in different environmental conditions.

The use of drone assisted airborne magnetic survey using vector magnetometers was explored at Institut de Physique de Globe de Strasbourg (IPGS) in 2016. Use of a global navigation satellite system (GNSS) antennae, controller and a Barington Mag-03 vector magnetometer were used, in the surveying of an french aerial base [11].

Figure 2.2 shows the results of a magnetometer survey taken from 1m above the ground with spacings of 0.5m. This shows UAV drone Magnetometers surveys are possible, but detecting meteorites requires the drone to be much closer to the ground due to a metoerite's significantly smaller magnetic field.

## 2.4 Magnetometer

Magnetometers can be divided into scalar or vector magnetometers, depending on the way they measure a magnetic field. Scalar magnetometers measure the magnitude of a magnetic field, regardless of the vector of the magnetic field, while vector magnetometers measure the flux density value of a magnetic field in a direction relative to its sensor 3 dimensional orientation.



**Figure 2.2:** The results from a drone assisted magnetometer survey [11]

When comparing the two, vector magnetometers are significantly more versatile, as to produce accurate results, scalar magnetometers search in line with the environments ambient field, which severely reduces there search practicality.

## 2.5 Planar Magnetic Gradiometers

A planar magnetic gradiometer is a configuration of two horizontally aligned vector magnetometers some distance apart. Gradiometers offer the most promise when locating small, near surface anomalies such as meteorites, as not only are physically small, light they also require little power [19]. The difference between the sensor readings are taken, meaning they can operate with a high degree of sensitivity and immunity to fluctuations in the ambient field.

The success of planar magnetic gradiometers is dependent on the alignment of vector magnetometer sensors. If the sensors are not leveled, components of a magnetic field cannot be accurately measured. Therefore, sensor suite leveling is needed in order for drone assisted meteorite detection to be successful.

## 2.6 Mass Moment of Inertia

A body is defined as an object with definite size and shape, such that every body of mass has both a translational and rotational aspect of motion. For rotational motion, the measure of resistance that a body has to angular acceleration ( $I$ ), is known as the Moment of Inertia ( $M$ ) [13]. This relationship is shown as:

$$T = J\alpha \quad (2.1)$$



Where  $T$  = Torque

$I$  = Mass Moment of Inertia

$\alpha$  = Angular Acceleration

Moment of Inertia can be separated into three aspects of rotational motion, about the X, Y and Z axis. This is known as the Roll, Pitch and Yaw of an object. To calculate the moment of Inertia, the area perpendicular to the axis of the object which is rotating around is used. The Mass moment of inertia can be found by separating the area into infinitesimal parts and adding them, which is represented in mathematical form as an integration. When dealing with objects of non-uniform density, the equation becomes more difficult. A table of simple shapes and their moment of Inertia formulas can be found below in Table 2.1.

Shape	$I_x$	$I_y$	$I_z$
Rectangle	$\frac{m(l^2+h^2)}{12}$	$\frac{m(h^2+w^2)}{12}$	$\frac{m(l^2+w^2)}{12}$
Sphere	$\frac{2}{5}mr^2$	$\frac{2}{5}mr^2$	$\frac{2}{5}mr^2$
Cylinder	$\frac{1}{12}m(3r^2 + h^2)$	$\frac{1}{12}m(3r^2 + h^2)$	$\frac{mr^2}{2}$
Thin Ring	$\frac{mr^2}{2}$	$\frac{mr^2}{2}$	$mr^2$
Slender Rod	$\frac{ml^2}{12}$	$\frac{ml^2}{12}$	0

Table 2.1: X,Y and Z axis inertia formulas for basic 3D shapes

### 2.6.1 Parallel-Axis Theorem

When a body is made up of two or more objects, each with a different centre of mass it becomes difficult to calculate the body's moment of inertia. The solution to this problem is through application of the parallel axis theorem. The theorem states if the moment of inertia of a body is known about an axis passing through the body's center of mass, then the moment of inertia can be calculated about a parallel axis by the addition of its inertia plus the multiplication of the body's mass times the distance between the two axis squared. In mathematical terms, this is represented by:

$$I = I_G + md^2 \quad (2.2)$$

Where  $I$  = Inertia of the body at the parallel axis

$I_G$  = Inertia of the body at the body's center of mass

$m$  = Mass of the body

$d$  = Distance between the two axis'

When the object is made up of many different composite bodies, the moment of inertia can be solved by the addition of each composite bodies moment of inertia at the objects center of mass.

$$I = \sum I_G + md^2 \quad (2.3)$$

### 2.6.2 Roll, Tilt and Pan

A rotation of a body around its x, y or z axis is known as an object's roll, pitch and yaw. For camera control, rotational change is described as a change in roll, tilt and pan. Figure 2.3 illustrates the three motors of the Feiyu MG Lite gimbal, and how each motor controls an extra degree of rotational movement of the mounted object.

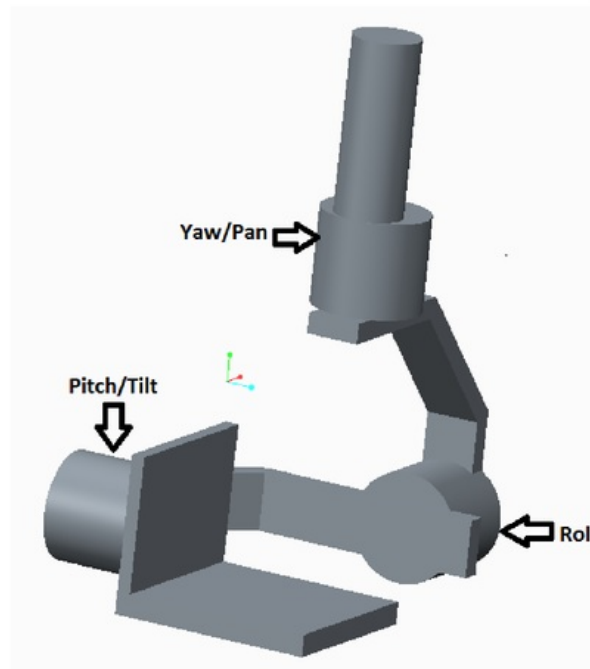


Figure 2.3: CAD of the Feiyu MG Lite

## 2.7 Signals and Modern Control Theory

Modern Control Theory is the study of the behavioural relationship between a system's input and its output. A system's characteristics can be explained by the Overshoot,  $T_s$  and SSE of the systems output to a simple step input.

Term	Definition
Transient Response	The response of a system with respect to time before it reaches its final value
Steady State (Continuos Response)	The value that the output achieves after all constituents of the transient response have faded
Oscillation	A periodic fluctuation between two things
$\zeta$ (Damping ratio)	A measure of how fast the reductions in amplitude of vibrations and oscillations
Peak	Highest amplitude of a waves period
Trough	Lowest amplitude of a waves period

**Table 2.2:** Definitions of Signals and Control Theory Terms

### 2.7.1 Step Input

A step input is an input wave that instantaneously jumps from its original position to its final value.

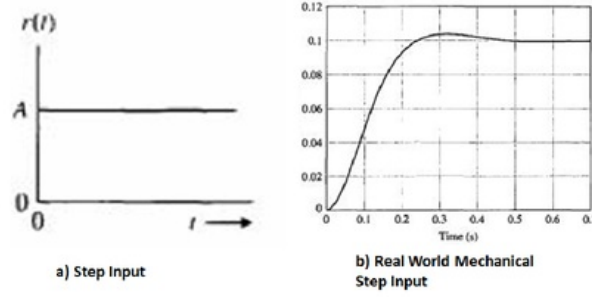
#### Real World Step-Input

In the real world, an instantaneous jump from the original position to the final position is not possible. Therefore, when simulating a mechanical movement, overshoot and oscillation often occurs. A representation of a mechanical real world step input is depicted in Figure 2.4. Inputs with a short rise time and little overshoot and oscillation are preferred, as the characteristics of a system become less clear the more noise in the input wave.

### 2.7.2 Output Response

The output of a system is the response of the system to an input wave. In control theory the response of that wave is measured in terms of Percentage Overshoot, Settling Time and Steady State Error, as seen in 2.5.





**Figure 2.4:** Comparison of theoretical and real Step Inputs [7]

### Percentage Overshoot

Percentage Overshoot, is defined as the percentage that the response wave initially overshoots the final value of the response [7]. This can be represented numerically as:

$$P.O = \frac{M_{pt} - fv}{fv} \times 100\% \quad (2.4)$$

Where  $M_{pt}$  is the peak value of the time response  $fv$  is the final value of the response

### Settling Time ( $T_s$ )

The Settling Time,  $T_s$ , is defined as the time for the system output to settle within a certain percentage  $\delta$  of the initial input amplitude [7]. In a Second-Order System,  $T_s$  can be represented in terms of its damping ratio ( $\zeta$ ) and natural frequency ( $\omega_n$ ). Figure 2.5 shows the time to which a response would settle within  $x\%$  of the initial input amplitude.

$$T_s = \frac{-(\log_e x\%)}{\zeta\omega_n} \quad (2.5)$$

Where  $\zeta$  is the damping ratio and  $\omega_n$  is the natural frequency

### Steady State Error ( $SSE$ )

The SSE is the error of the continuous response that remains after the transient response of the signal has disappeared [7]. The  $SSE$  of a system can be defined as:

$$E(s) = R(s) - Y(s) \quad (2.6)$$

Where  $E(s)$  is the error of the continuous response  $R(s)$  is the desired output  $T(s)$  is the actual output.

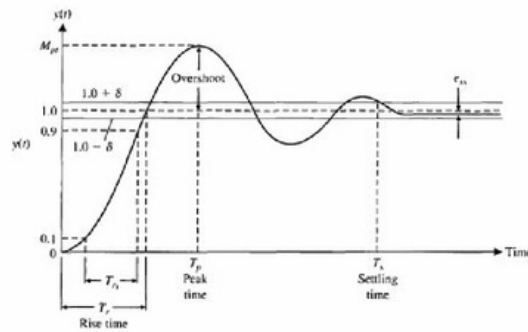


Figure 2.5: Unit Step Response [7]

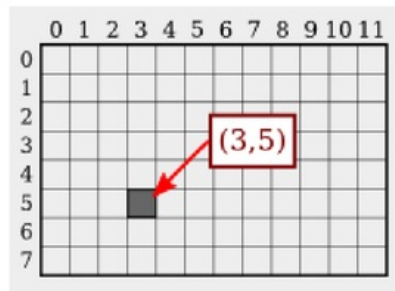


Figure 2.6: Pixel coordinates [8]

### 2.7.3 Image Pixel Co-ordinates

In an image, a user space coordinate system is used, where the origin (0,0) lies at the top left hand corner of the image. Pixels are represented using x,y co-ordinates, where x-co-ordinates increase towards the right of the image, and the y-coordinates towards the bottom of the picture. This is illustrated in Figure 2.6.

# Chapter 3

## Project Methodology

### 3.1 Methodology Introduction

This section looks to outline the methodology and testing procedure that was adopted for the use of accomplishing the projects goal specified in Section 1.3.1. To accomplish the aims and goals of the project, the project was divided into three phases.

Phase one involved the attachment of the sensor suite to the gimbal, and the gimbal's ability to function under the load of the sensor suite. Changes to the weight of each side was added in this phase, in an attempt to produce a horizontal sensor suite when the gimbal is at rest.

Phase two involved the design and construction of the testing apparatus designed to mimic the movement of a drone's step change in roll. This included the design and construction of a lever apparatus capable of a  $0 - 25^\circ$  tilt.

Lastly, Phase three looked into the methods used to capture the gimbal's response to the step change in angle via high speed camera footage, and image processing software used to analyse the gimbal's characteristic response.

## 3.2 Phase One

Phase One of the project included the calculation of the sensor suite's moments of inertia, the gimbal selection and the mounting of the sensor suite to the gimbal.

### 3.2.1 Resource Requirements

To complete this phase of the project, the required resources used included:

1. Gimbal
2. Sensor Suite
3. Mounting Device
4. Gimbal Software
5. Adjustable Weight System

### 3.2.2 Moments of Inertia of the Sensor Suite

The sensor suite was made up of many different bodies. Therefore, to determine the moment of inertia of the sensor suite, the moment of inertia for each body as calculated by weighing the body, and applying the parallel axis theorem method described in 2.6.1. Summing the results from each body, the moment of inertia for the sensor suite's roll, pitch and yaw axis was found.

As the sensor suite parts had been glued together by the Geology department, rough estimations and assumptions were made. The sensor suite was assumed to be made up of three basic objects. These included the sensor suite arms, the sensors and the middle connector piece.

To determine the weight of each object, the mass of the sensor suite was measured first. Then the sensor piece was unclipped from the sensor suite and weighed. To determine the weight of each sensor arm, an off-cut of the material was located, and then by finding the mass density of the object, the mass for the sensor arm was calculated. The weight of the wires inside each sensor arm were also compensated for, by weighing an offcut of wire, and using the same technique. The weight of the wire was accounted for in the calculations of the sensor arm. Finally the weight of the connector piece was found by subtracting the mass of the other parts from the total weight of the sensor suite.

For the calculations of the moment of inertia of the sensor suite, the assumption was made that all bodies that make up the sensor suite, are uniform in density. The moment of inertia for the sensor suite was then found for each axis, shown in Figure A.2.

### 3.2.3 Gimbal Selection

Category	Ikan DS1 Beholder	Feiyu MG Lite
Price (Includes Shipping)	\$776.28	\$776.28
Weight (Kilograms)	1.1	0.887
Load Capacity	1.7	2
Supports Inverted	Yes	Yes
Range: Roll	355°	360°
Tilt	295°	: 360°
Pan	335°	360°
Increments: Tilting	N.A.	2 – 75°/s
Panning	N.A.	3 – 150°/s
Usage Time	4 Hours	6 Hours
USB Port	Yes	Yes
Review	3.5 stars	4.0 stars

**Table 3.1:** Comparison of Ikan DS1 and the Feiyu MG Lite Specs

### 3.2.4 Comparison

Comparing the Feiyu MG Lite against the Ikan DS1, the MG Lite comes with two distinct advantages over its competitor. The main advantage of the Feiyu, is its weight efficiency. Its ability to carry a higher load than the Ikan, while also weighing significantly less, means that the Feiyu can perform tasks requiring higher torque than the Ikan can, while being less of a weight burden on the drone.

The second big advantage that the Feiyu has over the Ikan, is its range and adjustment speed. Having the ability to reach its level state faster after changes in the roll, pitch and yaw of the drone is a great advantage in the project. This allows the sensors in the sensor suite to detect potential material quicker, meaning that the drone can fly at faster speeds thus covering more ground.

## 3.3 Feiyu Gimbal Software

The ability to change the gimbal's response to sudden shifts in roll, pitch and yaw is a great addition to the thesis. Feiyu offers users software in the form of an android app named Feiyu On, that allows for individual motor tuning.

### 3.3.1 Feiyu On

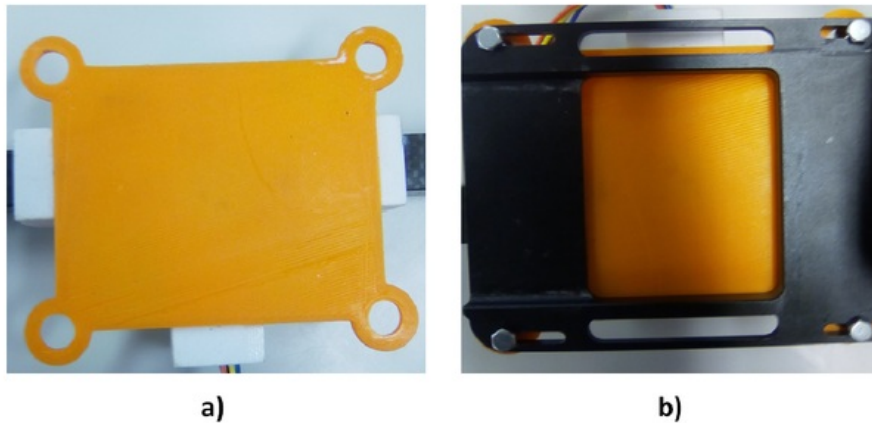
The Feiyu On is an app that allows for the control of simple factors of the MG Lite gimbal. The app allows the user to connect to the gimbal via bluetooth. Once connected the app gives users the ability to control simple functions of the device. However, control is limited to a very limited number of practical applications.

The MG Lite has three modes, lock, panning and tilting. This project utilised the lock mode, which allows for the device to remain in the original orientation as when the gimbal was originally turned on. This means that it will effectively compensate for sudden movements made by the testing apparatus or drone. This is accomplished through the feedback system of the MG Lites's gyroscope.

Another feature of the Feiyu On app, is its ability to customise motor strengths for the roll, pitch and yaw axis. This is essential in the project, as changing the tilt motor strength of the gimbal, will affect the characteristic response of the gimbal to the sudden change in roll. Analysing and comparing the response of the gimbal at different motor strengths allows for estimations of the PID system used in the Feiyu MG Lite.

### 3.3.2 Mounting the Sensor Suite to the Gimbal

An important part of phase one, was the attachment of the sensor suite to the gimbal. Because of the design of the gimbal and the length of the sensor suite, the sensor suite would need to be attached to the bottom of the gimbal camera holder. This has no effect on the sensor suite position, as the change in angle is identical as when it would be mounted on top of the gimbal holder.



**Figure 3.1:** a) Plastic Plate on top of sensor suite b) Sensor Suite attached to Bottom of Gimbal Camera Mount

Originally, it was proposed to design and print 3D piece that would allow the sensor suite to be attached to the sensor suite via screws, without damaging the structure of the sensor suite were contemplated. However, after obtaining the sensor suite from the Geology department, parts of the sensor suite were already glued together, with an additional plastic plate with four holes in each corner at the top shoown in Figure 3.1(a). The plate was deemed suitable, and so it was used, instead of trying to separate it from the sensor suite. Figure 3.1(b) shows the sensor suite mounted to the gimbal.

### 3.3.3 Variable Weight System

When attaching the sensor suite to the bottom of the gimbal, it was found that the gimbal rested at a slant, due to inertial difference or imperfect mounting. It is important that the sensor suite rests at a horizontal leveled position when the gimbal is off, as it makes the gimbal more effective in terms of response time, and power efficieny.



**Figure 3.2:** Attached Hose clamps for use of Weight system

For the design of the variable weight system, the weight required to level the sensor arm was calculated by attaching spare bolts to one end of the sensor suite until it was leveled. These spare bolts were weighed, and then hose clamps were used to replace them.

Part	Weight (grams)
Four Bolts	26
Hose Clamp	3
Bolt + Nut	3
<b>Weight of one Hose Attachment</b>	<b>12</b>

**Table 3.2:** Masses for the parts used in the weight system

Each Hose attachment included two hose clamps with two nuts and bolts. Two of these hose attachments were added to one side of the sensor suite, with a total weight of 24 grams. The attachments were placed at the end of the sensor suite arm, as shown in Figure 3.2.



## 3.4 Phase Two

Phase two of the project involved the design and completion of the simulation testing device.

### 3.4.1 Resource Requirements

1. Mounted Sensor Suite on MG Lite
2. Hafco MetalMaster DMF42
3. Mounted Door Hinge
4. 3 Pieces of Aluminum
5. Metal pole
6. 2 x U Bolt
7. M6 Nuts, Bolts and Washers
8. C83 Utility Extension Spring
9. Clamp
10. White labels
11. Black Marker
12. Sponge

### 3.4.2 Testing Device Requirements

In order to view and capture the characteristic response of the gimbal to changes in the drones roll, pitch and yaw, it was important to set up appropriate testing procedures. The test was required to simulate a sudden change in the movement in roll, such that the response of the tilt motor could be captured and measured. The change in angle should be reflective of a drones movement. A list of testing device requirements are outlined in section 1.3.3

### 3.4.3 Testing Device Construction

The construction of the lever testing device was completed using 8 steps.

#### Step One: Securing Door Hinge onto metal rod

Step One of the testing device construction, involved the selection of an appropriate door hinge and metal rod. Once selected, the hinge was mounted onto the metal piece.

To accomplish this, measured drill spots were marked before a drill press and a *4mm* drill bit was used to drill holes into the metal. The drill spots were marked by mounting the hinge onto the rod such that the inner edge of the door hinge lined up with the edge of the metal rod. When the door hinge was properly aligned, a marker pen was used to mark the rod, where the holes in the hinge were positioned. After drilling the marked locations, a 4mm nut, bolt and washer were used to secure the door hinge onto the metal rod.

#### Step Two: Creation of the metal frame

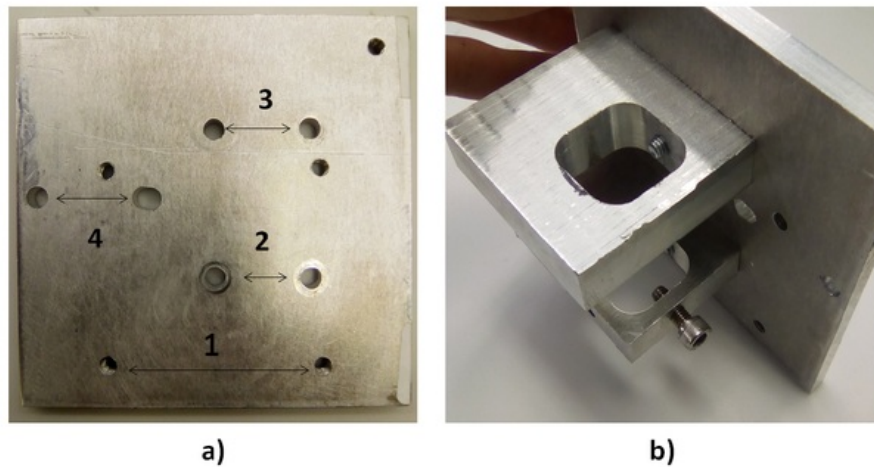
The metal frame piece was created by sawing through a sheet of aluminum. To refine the metal piece into the required dimensions and smooth the sides, the piece was milled into a 12x12cm aluminium square.

#### Step Three: Drilling metal frame

To mount the metal frame piece onto the hinge, a drill press was used to drill into the aluminum square frame. A total of four pairs of holes were drilled into the aluminum square frame shown in Figure 3.3. The holes marked 1 are for the attachment of the aluminum onto the hinge. Whilst 2 and 3 are for the perpendicular attachment of separate aluminum pieces. The holes marked 4 are used for the insertion of a U Bolt. All nuts and bolts used in this process are *M6*.

In order to create a correct fit, holes marked 1, were measured and marked with the door hinge before drilled into using the Hafco Metal Master Drill Press. A *5mm* drill bit was selected according to recommendations by a tap drill chart. The holes were then threaded using an *M6* tap.

Holes marked 2 and 3 in Figure 3.3(a) were drilled out using a *6.5mm* drill bit, to allow for the *M6* bolt to fit through the aluminium base plate and into the threaded aluminium pieces.



**Figure 3.3:** a) Aluminium Frame Plate b) Attached Aluminium Pieces to Frame Plate

#### Step Four: Milling Aluminum pieces

The next stage of the design construction, involved cutting appropriate sized hole in two selected aluminum offcuts seen in Figure ??(b). The holes needed to be wide enough to tightly fit the gimbal handle, which was measured to be  $2.79\text{cm}$  in diameter. A 16mm milling flute was used, in a repeated square movement pattern to cut a square hole through each aluminium piece.

To ensure that the pieces lined up when mounted perpendicular to the aluminium frame piece, the squares were cut  $5\text{mm}$  from the left side, and then the front sides were milled until the distance from the front to the hole was identical for both aluminium pieces.

#### Step Five: Drilling Aluminium pieces

To mount the aluminium pieces to the aluminium frame, M6 holes were drilled and threaded into the front side of the aluminium pieces. These holes were drilled at the same distance that holes marked 2 and 3 were on the Aluminium Frame.

An M6 hole was also drilled and threaded into the left side of one of the aluminium pieces, at the middle of the milled out square hole. This hole was used so that the M6 bolt would bite into the gimbal handle, securing it in place.

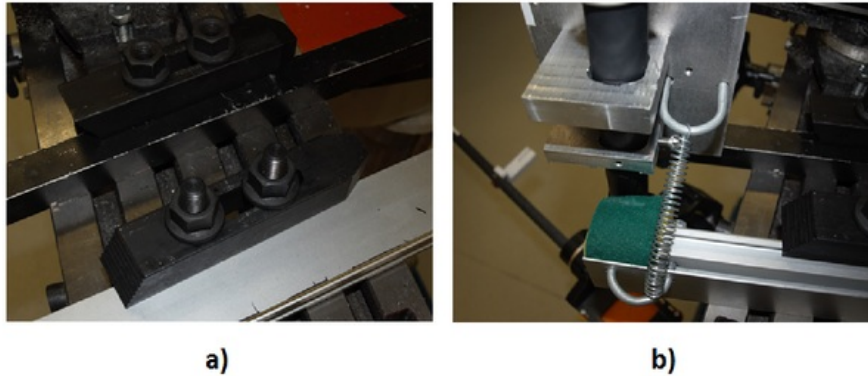
Subsequently, the aluminium pieces were mounted perpendicular to the aluminium frame (Shown in 3.3(b)) using M6 bolts, and washers.

**Step Six: Drilling into Metal Stopper**

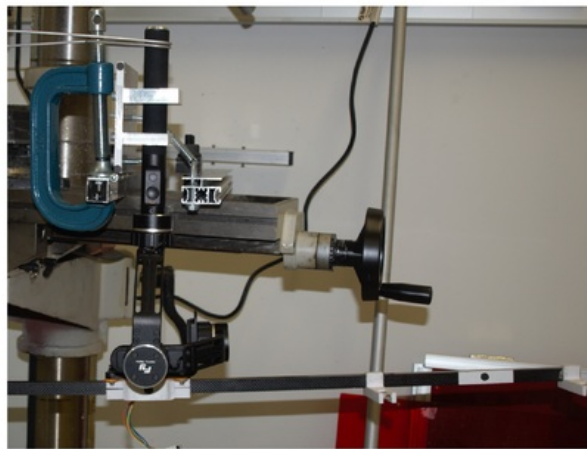
A metal stopper was chosen to stop the testing device at the desired angle. Holes were drilled into a stopper, to be used for the attachment of a u-bolt.

**Step Seven: Mounting onto drill press**

The testing device, and stopper were mounted onto a drill press (shown in Figure 3.4) slightly angled as to face the camera.



**Figure 3.4:** a) Mounted testing device. b) Attached Extension Spring and Sponge



**Figure 3.5:** Experiment Setup

**Step Eight: Attaching Extension Spring and Sponge**

After the metal pole and the stopper had been mounted onto the drill press, an extension spring was attached between the aluminium frame and the stopper. This served to pull the frame towards the stopper, reducing the rise time of the input.

A sponge was also attached onto the metal stopper between the contact area of the testing device and the stopper. This acted as a damping constant to the system, and reduced the severity of the oscillations and settling time.

## 3.5 Phase Three

Phase three outlines the methods used to capture and then image process the gimbal response to the simulated step input of the testing apparatus outlined in Phase Two.

### 3.5.1 Phantom Miro LC 320s

The Phantom Miro LC 320S is a high-speed camera that can capture up to 1320 frames per second at a 1920x1080 resolution with a 10um pixel size [4]. Its controls include record, trigger, trim, and playback and save to flash which can be executed via a flip-out LCD touchscreen or external monitor via 1GB Ethernet cable.

The memory of the LC 320S 6GB, can be segmented into many different partitions. This means, that the memory can hold several cines simultaneously.

The trigger can be adjusted so that it captures the events after, before or both when activated. In the case of this experiment, the trigger was set to save the 5 seconds captured before the trigger was activated.

### 3.5.2 Phantom Camera Control Software (PCC2.8)

Footage captured by the LC 320S was saved in Cine format on the external monitor using the Phantom Camera Control Software (PCC2.8). There the Cine was played and edited, so that only the test event was captured. This was accomplished by limiting the range of the frames, shown in Figure 3.6.

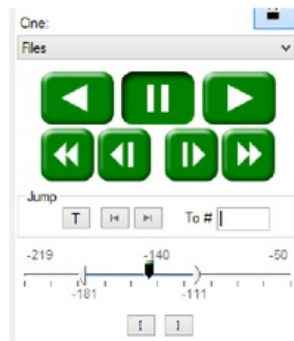


Figure 3.6: Cine Options

After editing was complete, the Cine was saved in a Multipage TIFF, so that the sequence of images could be image processed using ImageJ.

### 3.5.3 ImageJ Software

ImageJ software is an open source image processing program designed for multidimensional images [2], that permits the importation of an image or sequence of images, where users can scroll through the frames at will and filter images.

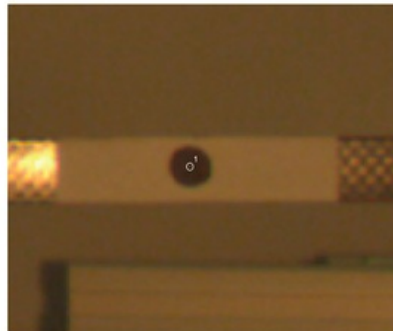
Two features and one plug-in were used in the process of editing the Cines from the PCC. The first was the zoom option, which allowed for the magnification of point of interest. By magnifying the point locations, the pixel accuracy of the data points was increased, as the user error decreased.

The second option used during the experimentation phase was the interval rate. The interval rate allowed for the specification of the time frame between each frame. When specified, data that is recorded will also have its time coordinate attached.

The Frame Interval option can be specified to nearest hundredth of a second. When conducting the test the LC 320s was shot at 180 frames per second, or 0.0056 seconds per frame. Therefore, when specifying the Frame Interval option, each frame interval was increased by a magnitude of 100 when measured in ImageJ, which was changed back in excel after the data was exported.

### 3.5.4 MTrackJ

MTrackJ is an ImageJ plugin to facilitate tracking of moving objects in image sequences [3]. The plugin allows the user to record the coordinates of an object at each frame, effectively tracking the object over a sequence of frames. Using the Add option on the MTrackJ user interface, users are able to click upon any location on the image. Upon doing so, the software then saved the pixel co-ordinates of the location as shown in Figure 3.7, and then ImageJ replaced the current frame with the next frame. By repeating the process, the objects changing coordinates were tracked over the images sequence.



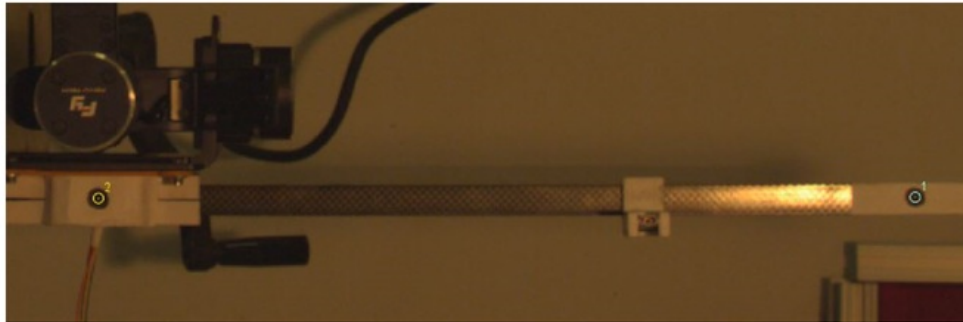
**Figure 3.7:** Saved Data Point



In the experiment phase MTrackJ options were used to increase work efficiency, ease of use and accuracy.

In the tracking tab, users are able to increase the frame skip in-between each save coordinates. During the image processing, the time step size was increased to 2 frames. As the event was captured at a high frame rate, tracking the object's movement every second frame was deemed adequate, as the loss in accuracy of the Gimbal Response, would be minimal.

The next feature used during the experiment was the display feature. The display allows users to display the reference point on the frame, and track over the sequence. During the image processing the highlighting of the reference was changed to white, so it was easier to distinguish against the black background of the dot. The track was customised such that active track was only shown after the last frame of the sequence had been referenced. This produced the most accurate results as displaying the active track often reduced visibility of the black dot.



a)



b)

**Figure 3.8:** a) Multiple point Tracking b) Finished Track



MTrackJ also enabled for the tracking of multiple objects in the same sequence, as shown in Figure 3.8(a). After finishing a track, the user is able return to the beginning of the sequence to start another track. Using this method, all four points were tracked sequentially, meaning data points from all four objects were exported collectively.

After the tracking of the four points, the data can be viewed using the measure feature on the user interface, shown in Figure 3.9(a). The data shows a number of different variables for each reference point, which are explained in table 3.9(b).

Nr	TID	PID	x [pixel]	y [pixel]	t [sec]
1	1	1	1696.833	985.5	0
2	1	2	1692.167	986.167	1.12
3	1	3	1686.833	985.5	2.24
4	1	4	1678.167	984.833	3.36
5	1	5	1668.833	984.833	4.48
6	1	6	1654.833	983.5	5.6
7	1	7	1636.833	982.167	6.72
8	1	8	1614.167	976.833	7.84
9	1	9	1589.5	970.833	8.96
10	1	10	1560.833	962.167	10.08
11	1	11	1531.5	949.5	11.2
12	1	12	1505.5	934.833	12.32

a) MTrackJ Measure Tab

Abbreviation	Definition
NR	The tracking number of the data point in the image
TID	The object tracking number
PID	The number of the data point in the object track
x [pixel]	The x-coordinate pixel of the object
y [pixel]	The y-coordinate pixel of the object
T[sec]	Time of the frame when the data was taken

b) Table of MTrackJ Measure Table Terms and Definitions

Figure 3.9: MTrackJ Measure Tab

From the measure feature, the data can be exported into excel, where it is possible to make calculate the angle between the reference points using the x and y pixel coordinates.

#### Angle between two points

To find the angle between two points, the tangent rule can be applied. The tangent rule states that the angle between two points from the horizontal is:

$$\begin{aligned}
 \tan \theta &= \frac{\text{Opposite}}{\text{Adjacent}} \\
 \tan \theta &= \frac{y_2 - y_1}{x_2 - x_1}
 \end{aligned}
 \tag{3.1}$$

where  $\theta$  = Angle between the two points

$y_a$  = y-pixel co-ordinate at point a

$x_a$  = x-pixel co-ordinate at point a

However, because of the method that pixel coordinates are referenced in images mentioned in Section 2.7.3 the polarity of the y-axis is reversed, and hence the polarity of the y values also changes. Therefore, the new equation can be written as:

$$\tan\theta = \frac{y_1 - y_2}{x_2 - x_1} \quad (3.2)$$

### 3.5.5 Accounting for Uncertainty

When collecting data points, there is a possibility for the presence of uncertainty caused by user error and image blur. To compensate, uncertainty can be calculated so that a range of angular values for the input wave and the gimbal response may be determined. To calculate the uncertainty for the angles of the gimbal handle and the Sensor Arm, the below Equations 3.3 and 3.4 were used.

Uncertainty in a Difference rule, used when two variables are being added or subtracted from one another, states that the total uncertainty of two measured variables, is approximately the sum of their uncertainties [20].

$$\delta q \approx \delta x + \delta y \quad (3.3)$$

Where  $\delta q$  = Total Uncertainty  
 $\delta x$  = Uncertainty of x variable  
 $\delta y$  = Uncertainty of y variable

Uncertainty in a Product, states, that when two variables are multiplied or divided, the total uncertainty is the sum of the variable's fractional uncertainties multiplied by the absolute value of the result [20].

$$\frac{\delta q}{|q|} \approx \frac{\delta x}{|x|} + \frac{\delta y}{|y|} \quad (3.4)$$

When calculating the angles of the input and response wave, an uncertainty was calculated by an error estimation of 2 pixels for each data point.

## Chapter 4

# Gimbal Response to Simulated Step-Response Experiment

### 4.1 Gimbal Response Introduction

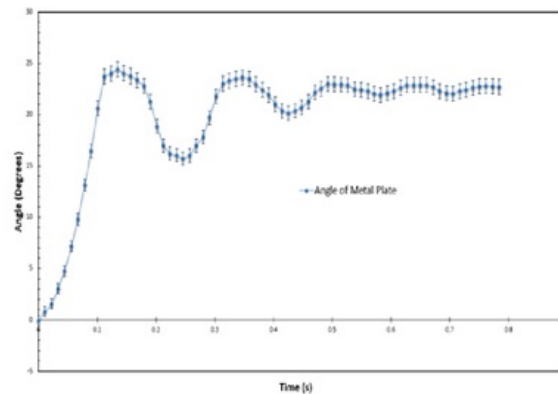
This chapter reports the results achieved from the Experiment. The results feature graphical representations of the Simulated step input, and the response of the Sensor Arm to the input wave. Results of Overshoot,  $T_S$  and  $SSE$  are defined, and displayed in a tabular form in this chapter.

### 4.1.1 Input Wave

When conducting the experiment, the input wave was calculated as the angle change of the Gimbal handle. By Tracking over time points 3 and 4, shown in Figure 4.1(a), an estimation of the input wave was calculated. Figure 4.1(b) shows the results from Tracking.



a) Tracked movement of Gimbal Arm in Exp3a



b) Angle change of Gimbal Arm in Exp3a with Uncertainty

Figure 4.1: Exp3a Gimbal Arm Angle Change

### 4.1.2 Failed tests

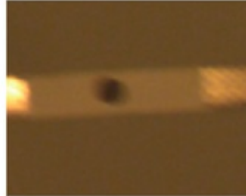
During the experiment phase a total of sixteen tests were conducted. Six of these tests were deemed failures. Five of these were as the initial sensor arm angle was deemed to be outside normal operating parameters, and one was because of the uncharacteristic input wave. Results collected from failed tests have been omitted, as they would skew the results and conclusion obtained from the successful tests. Table 4.1 Shows the success of each individual test.

	1	2	3	4
A		✓	✓	✓
B	✓			✓
C	✓			✓
D	✓		✓	✓

Table 4.1: Table of Successful Tests

### 4.1.3 Image Blur

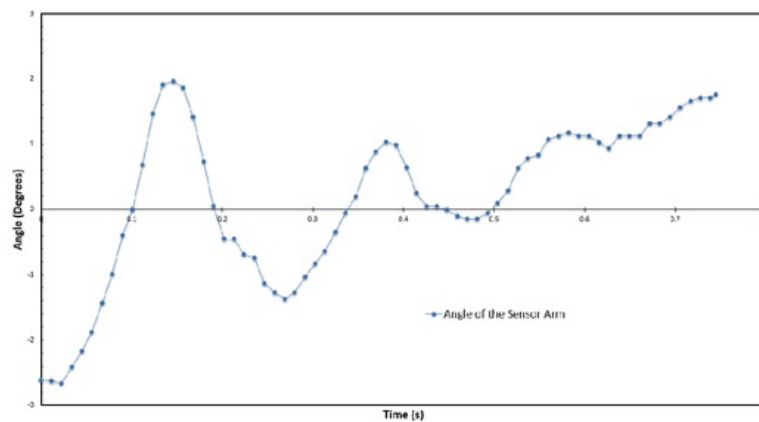
Images captured by the LC 320s were subject to after shadows due to the long exposure time of the camera. This effect, seen in Figure 4.2 increases the user error of data points when tracking an object. This in turn increases the uncertainty of some of the data points collected.



**Figure 4.2:** The after shadow effect on a frame

### 4.1.4 Drifting

During testing, the Sensor arm was subject to drifting at the end of the test. Drifting can be defined as a continued upward or downward movement of the Gimbal Response Angle, after the transient response of the signal has disappeared. Figure 4.3 shows drifting that occurred during Experiment 4b. The gimbal response follows the response of a characteristic second order response system, before a continued upward angle movement occurs at approximately 0.55 seconds.



**Figure 4.3:** Drift upward of the Sensor Arm in Exp4b

### 4.1.5 Response Wave Overshoot

Overshoot is usually measured as a percentage defined in Section 2.7.2. However, as the desired response is for the output to return to zero, it is more appropriate to define overshoot as a magnitude. In this section, overshoot is defined as the difference between the First wave peak angle and initial angle of the Gimbal Response.

### 4.1.6 Response Wave Settling Time

For the same reasons stated in 4.1.5, the response  $T_s$  is also defined using a magnitude. In this section, two definitions for settling time were calculated.  $T_s$  was calculated as the time required for the system to settle within  $1^\circ$ , and  $0.5^\circ$  of a settling angle.

As not all response waves settled towards  $0^\circ$ , it was important that a settling angle be established for each test. When deciding a settling angle for each test, there were three cases to consider. That the response wave:

1. Settles towards  $0^\circ$ .
2. Settles towards a settling angle that is not  $0^\circ$ .
3. Does not settle, due to drifting.

For case 2, the settling angle was set as an approximation of the response's limit as time increases. For case 3, a settling angle was set as an approximation of the response's limit before drifting occurred.

### 4.1.7 Response Wave Steady-State Error

For this experiment,  $SSE$  was defined according to Section 2.7.2. That is that  $SSE$  is equal to the difference between the settling angle and the final Response angle. Tests that were subject to drifting, were omitted from  $SSE$ .

## 4.2 Experiments

In total, sixteen experiments were conducted. Tests were taken under four varying conditions, with four tests conducted under each set of conditions. Two controlled variables were used during testing. These included the simulated angle change of the testing device, and the load applied on the gimbal mount. Table 4.2 illustrates the conditions that each tests were taken under.

Experiment Number	Simulated $\angle^\circ$	Centered Mass (Kg)
1a-1d	25	0
2a-2d	25	0.2
3a-3d	20	0
4a-4d	20	0.2

**Table 4.2:** Condition of Tests

### 4.2.1 Experiment One

Experiment One was taken under no extra load conditions, and a simulated angle of  $25^\circ$ . Under these conditions, three tests were successful. The results of the successful tests from Experiment One, can be seen in Table 4.3.

Exp No.	Init. $\angle^\circ$	Overshoot $^\circ$	$T_s < 1^\circ(\text{s})$	$T_s < 0.5^\circ(\text{s})$	Ref $\angle^\circ$	SSE $^\circ$
Explb	-2.49	3.70	0.41	0.44	-2	0.18
Explc	1.19	3.56	0.44	0.58	0	-0.24
Expld	0.77	3.52	0.43	0.45	0	
<b>Explavg</b>	<b>-0.17</b> $\pm 2.01$	<b>3.59</b> $\pm 0.09$	<b>0.43</b> $\pm 0.02$	<b>0.49</b> $\pm 0.08$		<b>-0.03</b> $\pm 0.30$

**Table 4.3:** Results from Experiment One

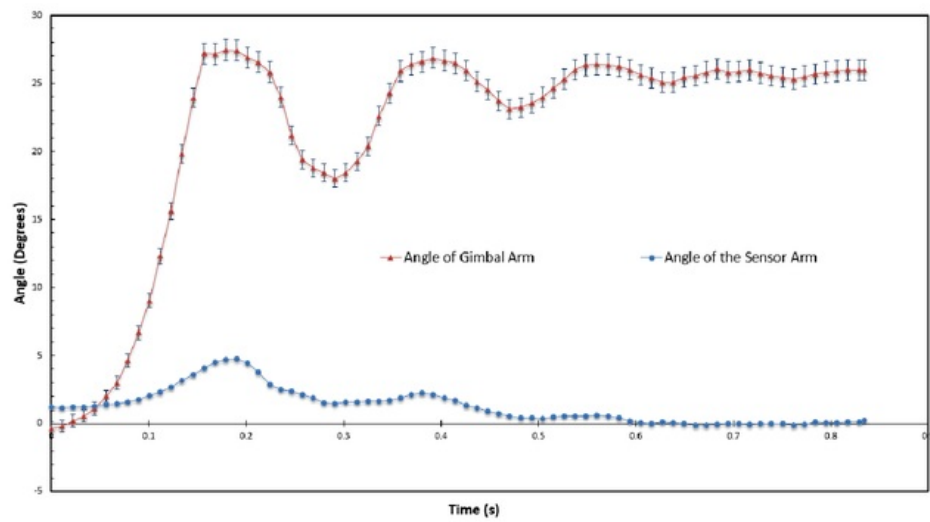


Figure 4.4: Exp 1c Simulation

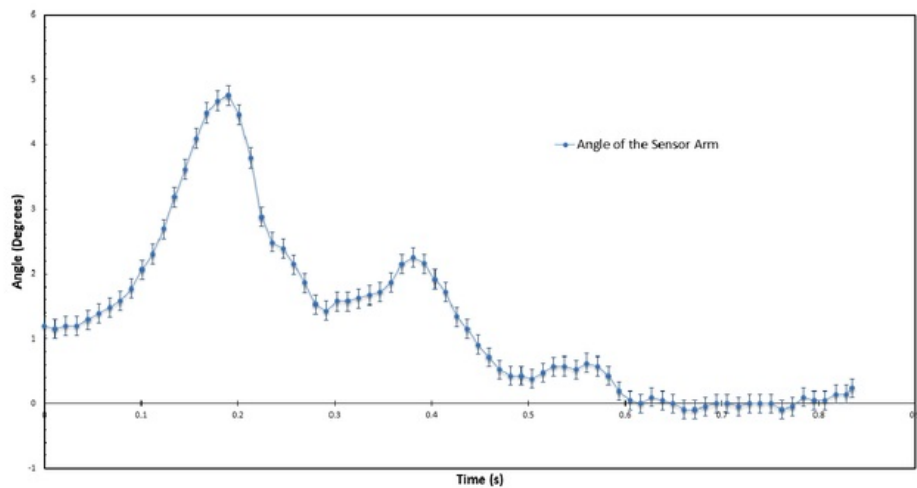


Figure 4.5: Exp 1c Response



### 4.2.2 Experiment Two

Experiment Two was taken under added load conditions, and a simulated angle of  $25^\circ$ . Under these conditions, only one of the tests were successful. The results of the successful tests from Experiment Two, can be seen in Table 4.4

Exp No.	Init.< ( $^\circ$ )	Overshoot( $^\circ$ )	$T_s < 1^\circ$ (s)	$T_s < 0.5^\circ$ (s)	Ref < ( $^\circ$ )	SSE( $^\circ$ )
Exp2a	-2.06	5.40	0.55	0.57	1.50	-0.15
Exp2avg	<b>-2.06 <math>\pm</math> 0</b>	<b>5.40 <math>\pm</math> 0</b>	<b>0.55 <math>\pm</math> 0</b>	<b>0.57 <math>\pm</math> 0</b>		<b>-0.15 <math>\pm</math> 0</b>

**Table 4.4:** Results from Experiment Two

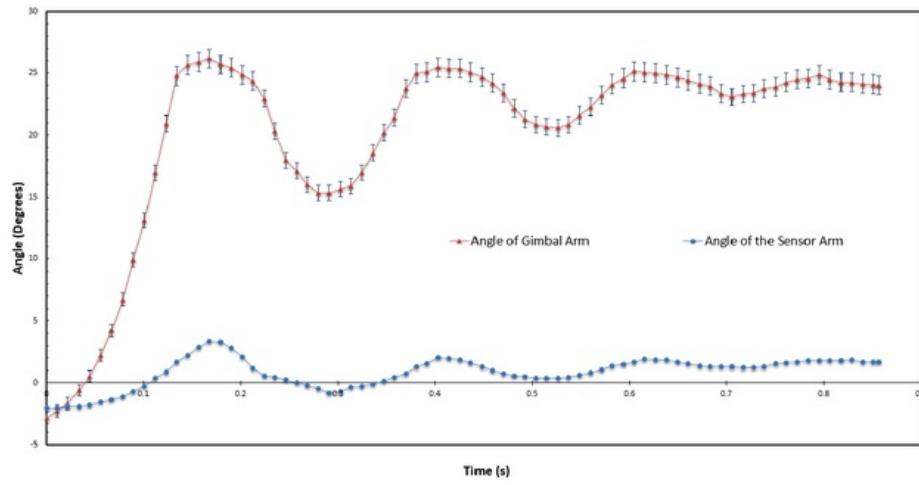


Figure 4.6: Exp 2a Simulation

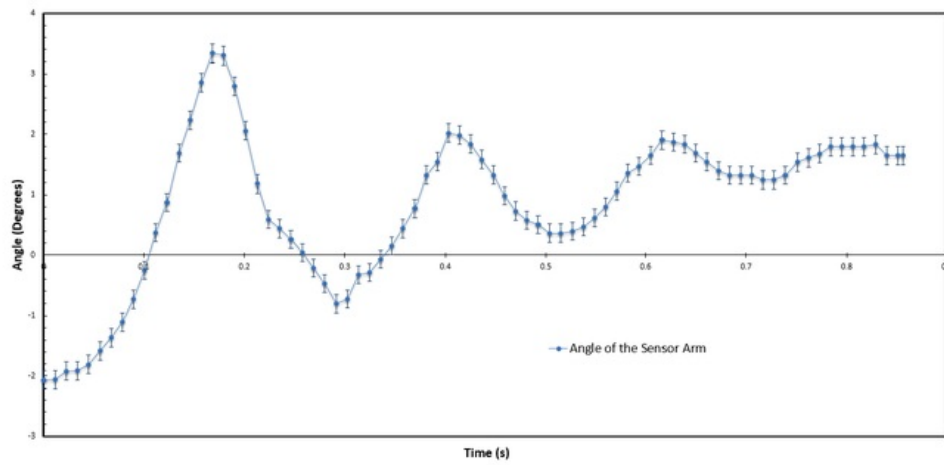


Figure 4.7: Exp 2a Response

### 4.2.3 Experiment Three

Experiment Three was taken under no added load conditions, and a simulated angle of  $20^\circ$ . Under these conditions, two of the tests were successful. The results of the successful tests from Experiment Three, are recorded in Table 4.5

Exp No.	Init.< ( $^\circ$ )	Overshoot( $^\circ$ )	$T_s < 1^\circ(\text{s})$	$T_s < 0.5^\circ(\text{s})$	Ref < ( $^\circ$ )	SSE( $^\circ$ )
Exp3a	0.17	3.17	0.37	0.38	0	0.07
Exp3b	0.10	3.68	0.39	0.68	1	-0.19
<b>Exp3avg</b>	<b>0.14</b> $\pm 0.05$	<b>3.43</b> $\pm 0.36$	<b>0.38</b> $\pm 0.01$	<b>0.53</b> $\pm 0.21$		<b>-0.06</b> $\pm 0.18$

**Table 4.5:** Results from Experiment Three

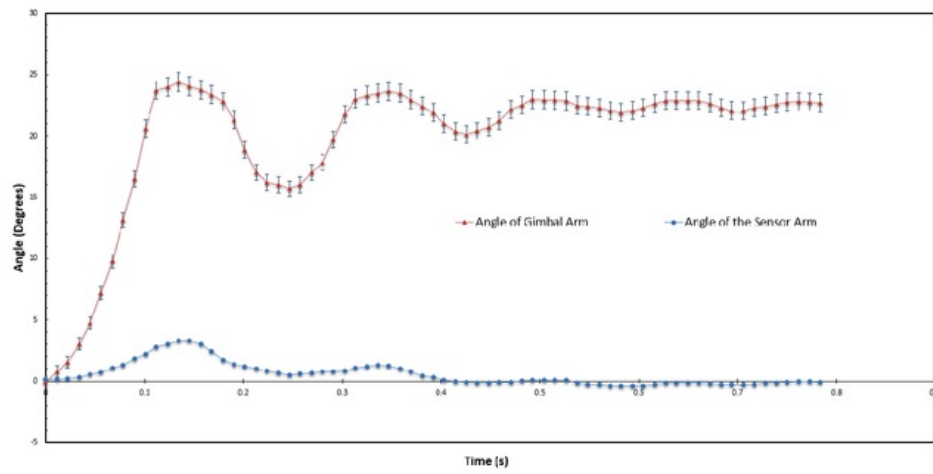


Figure 4.8: Exp 3a Simulation

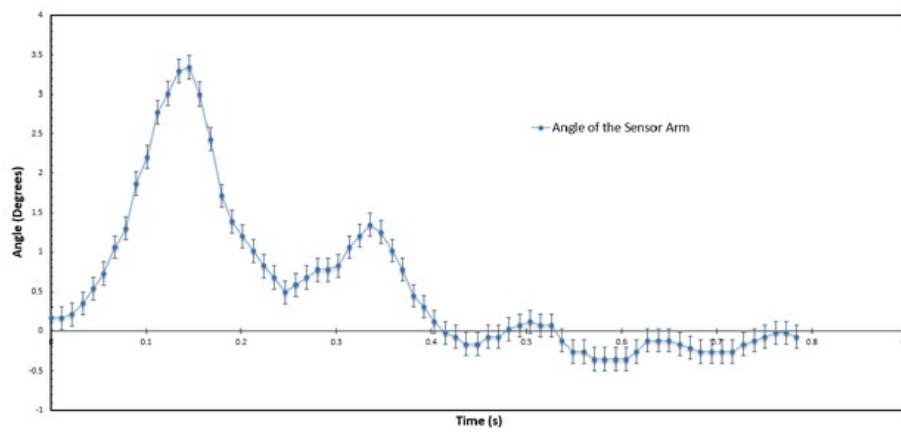


Figure 4.9: Exp 3a Response

#### 4.2.4 Experiment Four

Experiment Four was taken under added load conditions, and a simulated angle of  $20^\circ$ . Under these conditions, all four of the tests were successful. The results of the successful tests from Experiment Four, can be seen in Table 4.6

Exp No.	Init.< ( $^\circ$ )	Overshoot( $^\circ$ )	$T_s < 1^\circ(\text{s})$	$T_s < 0.5^\circ(\text{s})$	Ref < ( $^\circ$ )	SSE( $^\circ$ )
Exp4a	-2.60	4.59	0.31	0.51	0	-0.47
Exp4b	-2.61	4.57	0.31	0.51	0.5	
Exp4c	-3.25	4.96	0.32	0.39	0	
Exp4d	-3.45	4.28	0.31	0.49	-0.5	
<b>Exp4avg</b>	<b>-2.98</b> $\pm 0.44$	<b>4.6</b> $\pm 0.28$	<b>0.32</b> $\pm 0.01$	<b>0.48</b> $\pm 0.06$		<b>-0.4653</b> $\pm 0$

**Table 4.6:** Results from Experiment Four

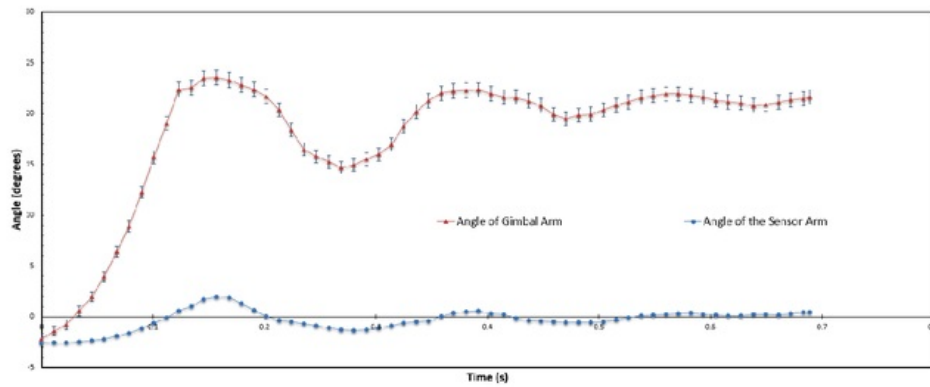


Figure 4.10: Exp 4a Simulation

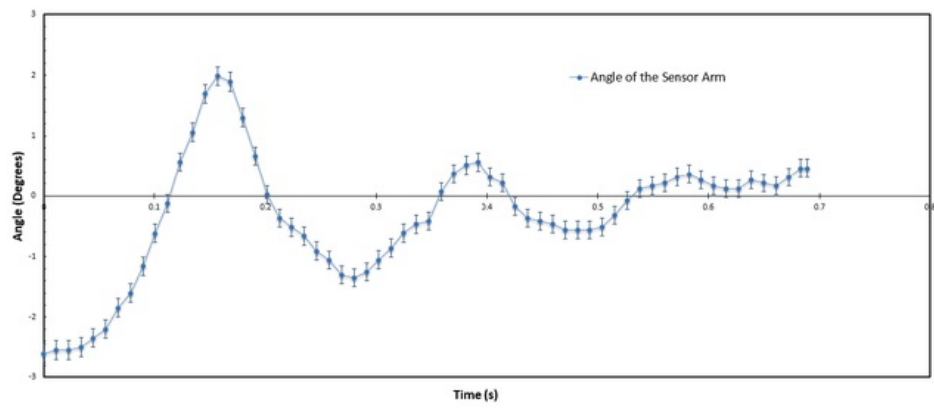
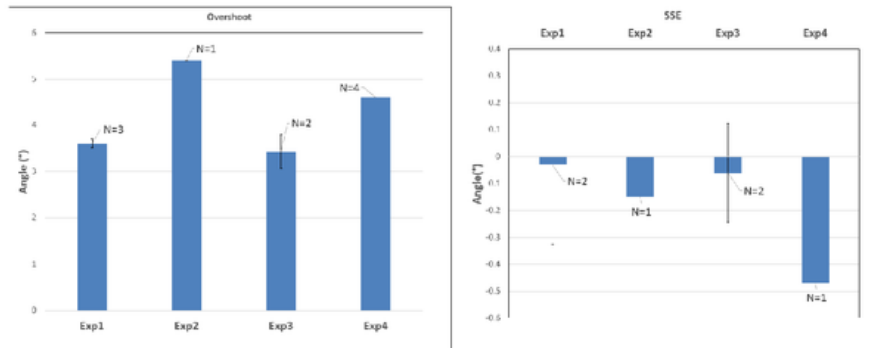
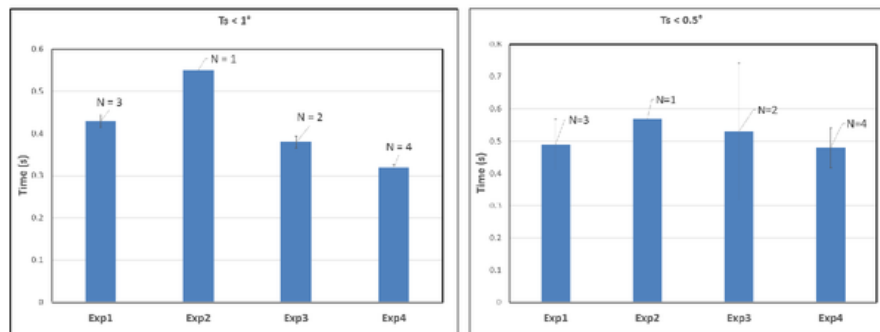


Figure 4.11: Exp 4a Response

### 4.3 Results



**Figure 4.12:** Bar Graph of Experiment Overshoot and Steady State Error



**Figure 4.13:** Bar Graph of Experiment Settling Time





# Chapter 5

## Discussion

### 5.1 Broken Roll Motor

During experiments, it was observed that the roll gimbal motor would only actuate in the counter-clockwise direction. This meant that during testing the tilt motor was only actuating when the sensor arm angle was approximately zero or below. Analysing the angle of the sensor arm in each of the experiments, it can be seen that when the arm angle drops below zero, the gradient of the response curve decreases. This is most evident in Experiment 4a between the curves first peak and trough in Figure 4.11. Due to this effect, the peaks of the gimbal's response are much steeper and higher than the troughs, indicating that the gimbal is only trying to correct the change in displacement of angle in the negative phase of the period.

### 5.2 Effect of Input wave

The initial overshoot and then damping oscillatory nature of the step input wave, means that the response settling time from the input wave is higher than if the input wave was an instantaneous step change. As the angle of the sensor arm is a response to the input wave, the longer it takes for the input wave to reach its continuous state, the longer it will take for the response to reach its continuous state. This means that the settling time of the response gets longer, as the settling time of the input gets longer.

The input wave also features troughs with greater amplitude than the peaks. This is to be expected, as the testing device, cannot go beyond the physical stopper, while the troughs are determined by the strength of the extension spring. This could also be a contributing factor as to why some response waves feature longer trough phases than peak phases per period.

### 5.3 Effect of Mass on the Gimbal's Response

When comparing Experiments 1 and 3 to Experiments 2 and 4 in Figure 4.12, an increase in mass can be seen to have a statistically significant positive effect on the overshoot of the gimbal response for both angle inputs. This is to be expected as when the lever is released there is a sudden change in the position of the sensor suite. The inertia caused by this sudden movement, causes the sharp increase in the angle of the sensor arm seen in the results. When the extra mass is added, the inertia of the sensor suite also becomes greater, causing a higher overshoot.

With a higher overshoot, the settling time should also increase, as damping of the response's higher peaks and lower troughs should take longer. However, as seen in Figure 4.13, there is no evidence to suggest this.

The lack of relationship between mass and settling time can be explained when comparing the waveform of Experiments 1 and 3 to Experiments 2 and 4. In Experiments 2 and 4, the response reacts as an under damped second order response oscillating around the settling angle, before settling on it. In Experiments 1 and 3 the response overshoots, before approaching the settling angle in a bumpy decline.

Analysing the response of Experiments 1 and 3, the sensor arm angle doesn't cross the  $0^\circ$  angle before the motor actuates, causing a bump during the curves decline. This reaction is potentially caused by the PID system in the gimbal. The roll accelerometer reads the downward acceleration of the sensor arm and tells the roll motor to actuate. As the motor is designed to level a camera, which has a significantly greater and more centralised mass than the sensor suite, the motor overcompensates, producing the results seen in Figure 4.5.

As the increase in mass is centralised, it theoretically should have no effect on the resting inertia of the load, and therefore no effect on the steady state error. Any inertial effect that the 0.2kg mass does have on the resting state, should be compensated by the strength of the roll motor.

Figure 4.12(b) results show that there may or may not be a statistically significant negative relationship between the mass attached and the SSE angle. This means that an increase of mass at the centre of the gimbal leads to a larger negative SSE.

This is hard to evaluate as the Steady State Error had a small sample size. Experiments 1 and 3 have sample sizes of 2, with high standard deviations. The comparison of these two experiments, show that there is little evidence of a relationship between extra mass and the Steady State Error of the response. Experiments 2 and 4 have a sample size of 1 due to Experiment 4 suffering from drifting and support the hypothesis that there is a statistically significant result between mass and the response's Steady State Error.

Looking closely at Experiment 4a's response in Figure 4.11, it can be seen that the response suffered from a less severe form of drifting for the last three data points, as they go above the previous periods peak. Therefore a more realistic result for Experiment 4 would be the angle of the last data point before drifting occurs, where the sensor arm angle is  $0.17^\circ$ . This would mean that both Experiments 2's and 4's results lie close to the results of Experiments 1 and 3 and therefore no evidence of a relationship between mass and Steady State Error would exist.

## 5.4 Effect of Angle change on Gimbal's Response

A greater step change in angle should cause a greater overshoot and settling time if the top speed of the step change has not already been reached. This is due to the inertial reasons stated in 5.3. This is reflected for overshoot in Figure 4.12(a) when comparing Experiment 2's and Experiment 4's results. For settling time, contradictory evidence supplied in Figure 4.13(a) and 4.13(b), suggests that there is a possible relationship between the amplitude of the change in angle and the settling time.

Factoring in the reevaluation of Experiment 4's SSE made in Section 5.3, there is no evidence to suggest that a relationship between the amplitude of the angle change and the gimbal response's SSE exists.

## 5.5 Gimbal's Response to movements in Pitch and Yaw

To accurately speculate the gimbal's response to movements in its pitch and yaw, the rotational inertia for each axis is needed. Looking at Figure A.2 in Appendix A the values for the moment of inertia for roll, pitch and yaw of the sensor suite are calculated.

From these results it can be shown that the moment of inertia about yaw is approximately equal to the moment of inertia about roll whilst the moment of inertia about pitch is significantly smaller than both roll and yaw. Therefore, it would be appropriate to surmise that a change in the drones yaw would produce a similar response to that seen in the drone's roll. For pitch, the overshoot and settling time would be significantly smaller, and the Steady State Error would be equal or less than that for the same degree of change in the drones pitch.



# Chapter 6

## Conclusion

This thesis investigated the ability of an off the shelf gimbal to horizontally level a sensor boom mounted to the bottom of a drone, based on the need for orientation sensitive packages to remain stabilized. Through simulations of the gimbals response to a drones movement in roll, using a lever device, the gimbal response's overshoot, settling time and steady state error with respect to varying centralised mass and amplitude of angle change were recorded and then calculated. Predictions on the effect of movements made in pitch and yaw, were made through the results from the roll experiments and calculations on the sensor suite's inertia.

Whilst testing, due to the roll motor malfunctioning, unpredictable initial angles, settling angles and drift occurred. Hence the amount of successful tests were low and the response featured inflated peaks.

Results proved that that there is a statistically significant relationship between the added centralised weight and the gimbal's response overshoot, and conflicting results for settling time showed that there is a possible a positive relationship between the amplitude of the angle change or added centralised mass and the settling time of the gimbal's response.

Results showed that a settling time within 0.5 degrees of the settling angle was achieved in a range of 0.3 to 0.7s. Steady state error was within 0.5 degrees of the settling angle. Accounting for statistical anomalies, the settling time range can be decreased from 0.4 to 0.55, and steady state error is within 0.2 degrees. With a working roll motor, both these values would be expected to decrease.

Drone movements in the yaw are predicted to have similar results as those seen in the roll direction, and the results of a movement in pitch would be predicted to have a smaller overshoot and settling time due to inertial differences of the sensor suite.

In conclusion, the findings of this thesis indicate that an off the shelf gimbal would provide a reasonably fast and accurate response to a drones change in roll, pitch or yaw. However, error from data retrieved from orientation sensitive loads, would be expected to occur during and up to 0.5s after the drone's movement.

## Appendix A

### Sensor Suite Roll, Pitch and Yaw Inertia

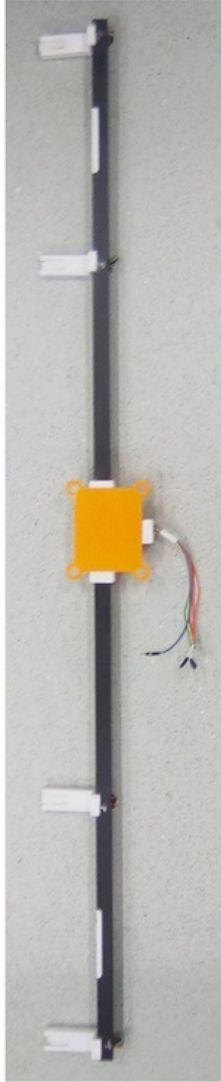


Figure A.1: Sensor Suite



Suite Inertia.png

Object Name	Width (Metres)	Length (Metres)	Height (Metres)	X-distance from Origin	Y-distance from Origin	Z-distance from Origin	Co-ordinates Center of Mass (X, Y, Z)	Mass (kilograms)	Roll Inertia	Pitch Inertia	Yaw Inertia
Pole 1	0.015	0.6625	0.015	0	0.35375	0	(0, -0.35375, 0)	0.06888	0.002686513	0.000005383	0.027057822
Pole 2	0.015	0.6625	0.015	0	0.35375	0	(0, 0.35375, 0)	0.06888	0.002686513	0.000005383	0.027057822
Connector Piece	0.024	0.095	0.024	0	0	0	(0,0,0)	0.12	0.0009501	0.0001152	0.0057025
Sensor 1	0.059	0.02	0.02	0.05	0.25	0.02	(0.05, 0.25, -0.02)	0.00887	0.002225176	0.000481479	0.00263716
Sensor 2	0.059	0.02	0.02	0.05	0.5	0.02	(0.05, 0.5, -0.02)	0.00887	0.00439138	0.000481479	0.004559421
Sensor 3	0.059	0.02	0.02	0.05	0.25	0.02	(0.05, -0.25, -0.02)	0.00887	0.002225176	0.000481479	0.00263716
Sensor 4	0.059	0.02	0.02	0.05	0.5	0.02	(0.05, -0.5, -0.02)	0.00887	0.00439138	0.000481479	0.004559421
Total								0.29324	0.067198465	0.001942602	0.068532166

Figure A.2: Roll, Pitch and Yaw Moments of Inertia of the Sensor Suite



# Bibliography

- [1] *Archaeological Geophysics for DoD Field Use: A Guide for New and Novice Users.*
- [2] *Image J.*
- [3] *MTrackJ: Manual.*
- [4] *PHANTOM MIRO M/LC CAMERAS MANUAL.*
- [5] A.W.R.Bevan, "Australian meteorites," *Records of the Australian Museum*, 1992.
- [6] B. S. Dimitros Apostolopoulos, Liam Pedersen, "Robotic antartic meteorite search: Outcomes," in *The Robotic Institute*, 2001.
- [7] R. Dorf and R. Bishop, *Modern Control Systems.* PEARSON, 2011.
- [8] D. Eck, *Introduction to Computer Graphics*, N.A, Ed. N.A, 2015.
- [9] L. Folco, P. Rochette, J. Gattacceca, and N. Perchiazzi, "In situ identification, pairing, and classification of meteorites from antartica through magnetic susceptibility measurements," *Meteorites & Planetary Science* 41, 2005.
- [10] A. Fossel, D. Apostolopoulos, and W. Whittacker, "Radar sensor for an autonomous antartic explorer," in *Robotics Institute*, 1998.
- [11] B. Gavazzi, P. L. Maire, M. Munsch, and A. Dechamp, "Fluxgate vector magnetometers: A multisensor device for ground, uav, and airborne magnetic surveys," *Institut de Physique du Globe de Strasbourg*, 2016.
- [12] R. Harvey, "The origin and significance of antartic meteorites," *Chemier der Erde Geochemistry*, 2003.
- [13] R. Hibbler and K. B. Yap, *Mechanics for Engineers DYNAMICS*, D. Villamero, Ed. PEARSON, 2012.
- [14] H. D. Jamie Pringle, "Forensic geophysics: Assisting law enforcement agencies in clandestine grave detection," *FastTIMES*, 2016.
- [15] L. of War, "Leftover unexploded ordnance (uxo)."

- [16] J. Paxman, P. Bland, R. Howie, M. Towner, M. Cupak, H. Devillepoix, and E. Sansom, "The desert fireball network: A sensor network for meteorite tracking and recovery," in *International Conference on Control, Automation, Robotics & Vision*, 2016.
- [17] L. Pedersen, M. Wagner, D. Aspostolopoulos, and W. Whittacker, "Autonomous robotic meteorite identification in antarctica," in *The Robotic Institute*, 2001.
- [18] L. Pederson, "Robotic deployment of electr-magnetic sensors for meteorite search," in *The Robotic Institute*, 1998.
- [19] G. Systems, "Advantages of magnetic gradiometers."
- [20] J. R. TAYLOR, *AN INTRODUCTION TO ERROR ANALYSIS THE STUDY OF UNCERTAINTIES IN PHYSICAL MEASUREMENTS*, A. MCGUIRE, Ed. University Science Books, 1982.
- [21] J. M. University, "Factsheets on landmines and uxo."
- [22] A. Wells-Dang, "A regional approach: Mine and uxo risk reduction in vietnam, laos and cambodia," *Journal of Conventional Weapons Destruction*, 2005.